AD-A095 954 NAVAL RESEARCH LAB WASHINGTON DC F/G 9/1
ANALYSIS OF THE WIDE BAND GYROTRON AMPLIFIER IN A DIELECTRIC LO--ETC(U)
MAR 81 J CHOE, H UHM, S AHN
UNCLASSIFIED NRL-MR-4460 NL

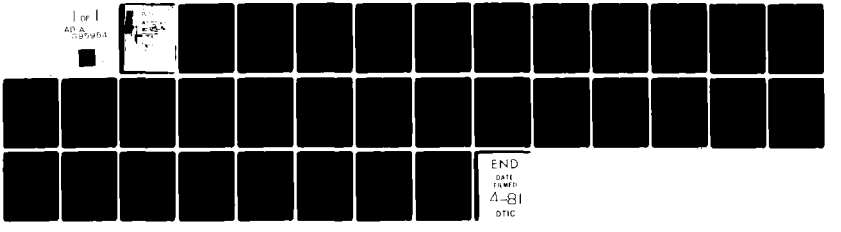

END
DATE FILMED
4-81
DTIC

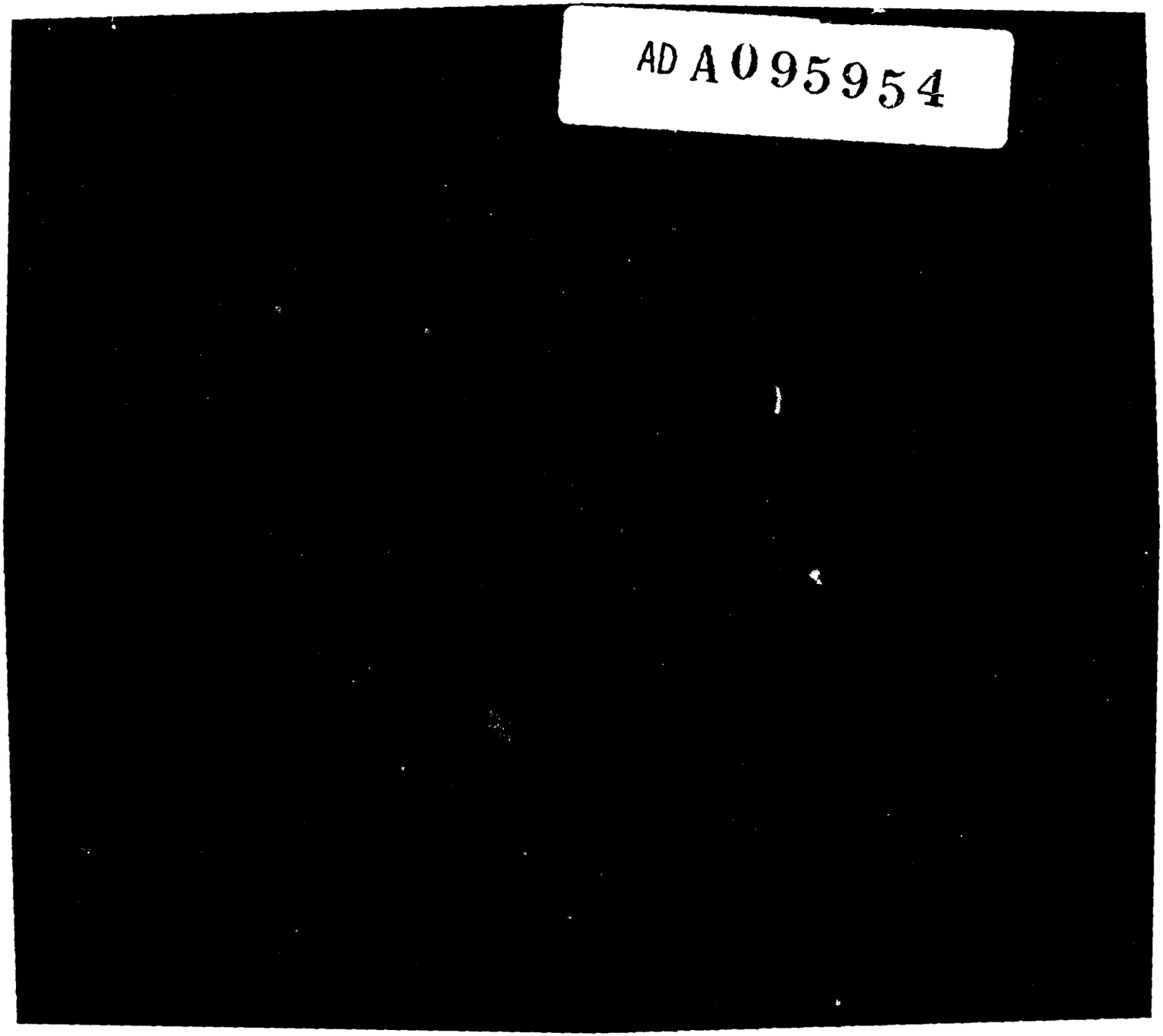

SECURITY CLASSIFICATION OF THIS PAGE (When Data Entered)

14 NRL-MR-4460

9 REPORT DOCUMENTATION PAGE

READ INSTRUCTIONS BEFORE COMPLETING FORM

1. REPORT NUMBER: NRL Memorandum Report 4460	2. GOVT ACCESSION NO. AD A095954
3. RECIPIENT'S CATALOG NUMBER	
4. TITLE (and Subtitle): ANALYSIS OF THE WIDE BAND GYROTRON AMPLIFIER IN A DIELECTRIC LOADED WAVEGUIDE	5. TYPE OF REPORT & PERIOD COVERED: Interim report on a continuing NRL problem.
	6. PERFORMING ORG. REPORT NUMBER
7. AUTHOR(s): J. Choe* H. Uhm* S. Ahn	8. CONTRACT OR GRANT NUMBER(s)
9. PERFORMING ORGANIZATION NAME AND ADDRESS: Naval Research Laboratory, Washington, DC 20375	10. PROGRAM ELEMENT, PROJECT, TASK AREA & WORK UNIT NUMBERS: 68-0755-0-1; NAVLEX; NSWC IR&D Funds
11. CONTROLLING OFFICE NAME AND ADDRESS: 12 34	11 12. REPORT DATE: Mar 81
	13. NUMBER OF PAGES: 33
14. MONITORING AGENCY NAME & ADDRESS (if different from Controlling Office)	15. SECURITY CLASS. (of this report): UNCLASSIFIED
	15a. DECLASSIFICATION/DOWNGRADING SCHEDULE

16. DISTRIBUTION STATEMENT (of this Report)

Approved for public release; distribution unlimited.

17. DISTRIBUTION STATEMENT (of the abstract entered in Block 20, if different from Report)

18. SUPPLEMENTARY NOTES

*Present address: Naval Surface Weapons Center, White Oak, MD.

19. KEY WORDS (Continue on reverse side if necessary and identify by block number)

Gyrotron
Cyclotron maser instability
Velocity spread
Slow wave structure
Dielectric waveguide
Wide band amplifier

20. ABSTRACT (Continue on reverse side if necessary and identify by block number)

The effect of broadening the bandwidth with a dielectric load in a cylindrical gyrotron is investigated for a hollow electron beam. The linear dispersion relation for the azimuthally symmetric, transverse electric (TE) modes is obtained by the method of the wave impedance matching. It is found that the TE perturbations exhibit three unstable modes characterized by their phase velocities (v_{ph}); one fast wave, the long wavelength mode (LWM, $v_{ph} > c$), and two slow waves, the intermediate (IWM, $c > v_{ph} > c\epsilon^{-1/2}$) and the short (SWM, $v_{ph} < c\epsilon^{-1/2}$) wavelength modes.

(Continues)

DD FORM 1 JAN 73 1473 EDITION OF 1 NOV 65 IS OBSOLETE S/N 0102-LF-014-6601

251950

SECURITY CLASSIFICATION OF THIS PAGE (When Data Entered)

20. Abstract (Continued)

The optimum conditions for the wide band operation are obtained individually for each mode. Although the bandwidth in excess of 40% is possible for the slow waves (IWM, SWM) at a small axial momentum spread, it decreases rapidly as the spread increases. On the other hand, the LWM yields approximately 10% of the bandwidth insensitive to the spread. It is also shown that for a small spread (< 5%), the slow wave (IWM) is preferable for the wide band operation, whereas for a large spread (> 5%) the fast wave (LWM) is desirable.

CONTENTS

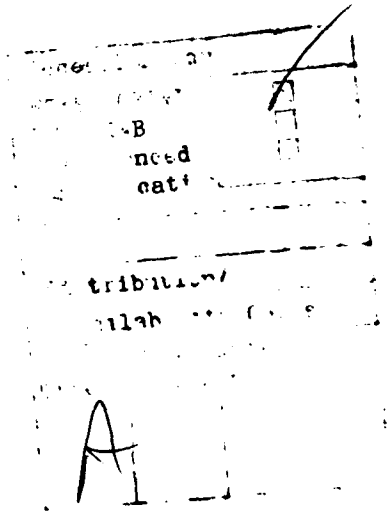

ANALYSIS OF THE WIDE BAND GYROTRON AMPLIFIER IN A DIELECTRIC LOADED WAVEGUIDE

I. INTRODUCTION

The gyrotron[1-3] is a high power microwave device that makes use of the Doppler-shifted electron cyclotron mode interacting with the waveguide mode. The appreciable microwave gain occurs only near the synchronous region between the waveguide and the beam modes. However, the bandwidth of a gyrotron in a perfectly conducting waveguide is very narrow. In order to broaden the bandwidth, it is necessary to slow down the waveguide mode by some slow wave structures[4] such as a dielectric load.[5-7] In this paper, we will examine the gyrotron in a dielectric loaded waveguide with the emphasis on increasing the bandwidth of instability.

The stability properties of the slow wave mode (or the intermediate wavelength mode, see Sec. III) in a rectangular waveguide have been previously studied, within the context of a fast rotational beam equilibrium.[5] However, in order to determine the optimum operational conditions in present experiments, it is necessary to investigate the gyrotron in a dielectric loaded, cylindrical waveguide. The purpose of this paper is to find a broad range of the optimum physical parameters in a wide band gyrotron operation, rather than to specialize some particular cases. In the process of the parametric investigations, we will identify all the unstable modes and will examine their characteristics by analyzing them individually in terms of a wide band operation.

The dispersion relation of the cyclotron maser instability is obtained by the method of the wave impedance matching,[8-10] without making use of the usual waveguide approximation for the perturbed fields.[11-13] In this regard, it is possible to predict not only the instabilities driven by the coupling of the waveguide-beam modes (the long and intermediate wavelength modes, see Sec. III), but also the instability driven by the highly

Manuscript submitted December 22, 1980.

localized fields at the beam location (the short wavelength mode, see Sec. III). Moreover, the influence of the axial momentum spread on the instability behavior as well as on the bandwidth of instability is investigated, assuming that the electron beam has a Lorentzian distribution in the axial momentum. It is found that the axial momentum spread plays a significant role in determining the bandwidth of instability.

The dispersion relation for the azimuthally symmetric, transverse electric (TE) mode is obtained in Sec. II utilizing the method of the wave impedance matching. In Sec. III, the resulting dispersion relation is examined and the three unstable modes are identified. We also investigate these three unstable modes individually in the next three sections, and the comparison of these modes for the wide band application with respect to the axial momentum spread is given in Sec. VII.

II. DISPERSION RELATION

We consider a cylindrical dielectric loaded gyrotron shown in Fig. 1. The dielectric material with its dielectric constant ε is filled from the inner radius $r = R_w$ to the conducting waveguide wall $r = R_c$. The beam electrons are gyrating with their Larmor radii r_L about their guiding centers at R_o. The electron beam is confined between $R_+ = R_o + r_L$ and $R_- = R_o - r_L$. We employ the cylindrical polar coordinates (r, θ, z) as shown in Fig. 1.

In order to make the problem tractable, we make use of the following assumptions:

(a) The theoretical analysis is described by the Maxwell-Vlasov equations for the electric and magnetic fields $\underset{\sim}{E}(\underset{\sim}{x}, t)$, $\underset{\sim}{B}(\underset{\sim}{x}, t)$, and the beam electron distribution function $f(\underset{\sim}{x}, \underset{\sim}{p}, t)$. Here $\underset{\sim}{x}$, $\underset{\sim}{p}$ and t refer to the space, the momentum and the time coordinates, respectively. Further, it is assumed that any quantity $\psi(\underset{\sim}{x}, t)$ can be linearized according to

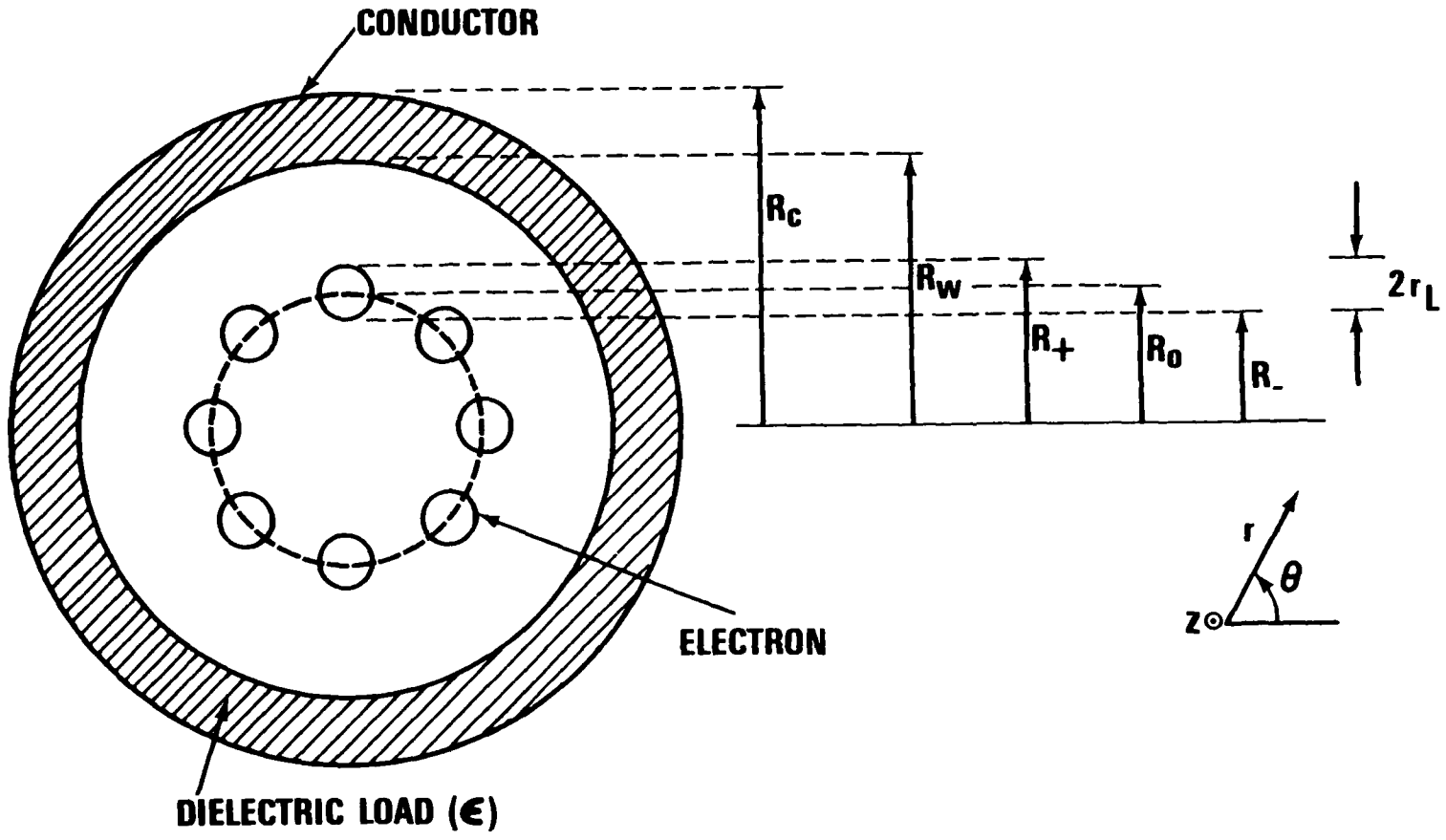

Fig. 1 — Configuration of a dielectric loaded gyrotron. A dielectric material is filled from its inner radius R_w to perfect conductor at R_c. The hollow electron beam is confined within $R_- < r < R_+$ with its center R_0.

$$\psi(\underset{\sim}{x}, t) = \psi_o(r) + \psi_1(r) \exp [i(kz - \omega t)], \tag{1}$$

with its equilibtium part ψ_o and the small perturbed quantity ψ_1. We explicitly assume that the equilibrium is symmetric in θ and z, and that the perturbation is azimuthally symmetric (i.e. $\partial / \partial\theta = 0$) with the frequency ω and the axial wave number k. Moreover, the present analysis is restricted to the transverse electric (TE) perturbation only (i.e., $E_{z1} = 0$).

(b) The electron beam density is assumed to be sufficiently small that the equilibrium self-field can be neglected. Specifically we assume that

$$\nu / \hat{\gamma} < < 1, \tag{2}$$

where $\nu = Ne^2/mc^2$ is Budker's parameter and $\hat{\gamma}\, mc^2$ is the electron energy. Here N is the total number of the electrons per unit axial length, and (-e) and m are the charge and the rest mass of the electron, respectively.

(c) Consistent with (a), it is assumed that the equilibrium fields are given by

$$\underset{\sim}{E}_o = 0, \ \underset{\sim}{B}_o = (0,0,B_o), \tag{3}$$

where B_o is the constant applied axial magnetic field strength.

(d) We also assume that the beam is very thin, that is

$$(R_+ - R_-)/R_o < < 1, \tag{4}$$

where $R_+ (R_-)$ is the outer (inner) boundary of the beam as shown in Fig. 1. Consistent with Eq. (4) we can approximate

$$R_+ \simeq R_o \simeq R_- . \tag{5}$$

(e) The equilibrium distribution function f_o, which is a function of the three invariants of the electron motion,[9,11] viz. the total energy γmc^2, the axial linear momentum p_z, and the canonical angular momentum P_θ, is

assumed to be

$$f_o = \frac{\omega_c \hat{p}_z \Delta}{4\pi^3 \hat{\gamma} mc^2} \; \delta(\gamma-\hat{\gamma}) \; \delta(P_\theta - \hat{P}_\theta) \; [(p_z-\hat{p}_z)^2 + \hat{p}_z{}^2\Delta^2]^{-1} \quad , \tag{6}$$

where $\hat{\gamma}$, $\hat{p}_z$, $\hat{P}_\theta$ and Δ are constants, and $\omega_c = eB_o/mc$ is the non-relativistic electron cyclotron frequency. Equation (6) describes the monoenergetic $(\hat{\gamma}mc^2)$ electron beam with the average axial velocity $c\beta_z = \hat{p}_z/\hat{\gamma}\, m$, the avergy transverse velocity $c\beta_\perp = c(1-\beta_z{}^2 - 1/\hat{\gamma}^2)^{\frac{1}{2}}$, and the average Larmor radius $r_L = c\beta_\perp/\omega_c$. We choose $\hat{P}_\theta = -eB_o(R_o{}^2-r_L{}^2)/2c$ to be negative so that the beam is hollow with its gyro-center at R_o. Moreover, the electron beam has a Lorentzian distribution in the axial momentum. The axial momentum spread is represented by $\hat{p}_z\,\Delta$ so that Δ refers to the axial momentum spread ratio. Compared to the thermal Maxwellian distribution[5] $f_o \propto \exp[-(p_z-\hat{p}_z)^2/(2\hat{p}_z^2\Delta^2)]$, it is found that

$$\Delta_{TH} \leftrightarrow 1.25\,\Delta \quad . \tag{7}$$

In terms of the spread influence, 4% of the Lorentzian spread is approximately equal to 5% of the thermal spread. Therefore, the Lorentzian spread Δ slightly overemphasizes the spread effect than the thermal spread Δ_{TH}.

The process of deriving the dispersion relation is identical to that of Uhm and Davidson[10] with one exception of the important modification of f_o with the axial momentum spread [Eq. (6)]. We therefore outline only the essential part, leaving out the details to that paper. The field equation for the azimuthally symmetric [Eq. (1)] TE perturbation is given by

$$\begin{aligned} B_{r1} &= -\frac{ck}{\omega} E_{\theta 1} \quad , \\ B_{z1} &= -\frac{ic}{\omega}\frac{1}{r}\frac{\partial}{\partial r}(rE_{\theta 1}), \\ \frac{\partial B_{z1}}{\partial r} &- \frac{i}{\omega c}(\omega^2\varepsilon_j - c^2k^2)E_{\theta 1} = -\frac{4\pi}{c} J_{\theta 1} \quad , \end{aligned} \tag{8}$$

where $\varepsilon_j = 1$ for $0 \le r \le R_w$ and $\varepsilon_j = \varepsilon$ for $R_w \le r \le R_c$. The perturbed current $J_{\theta 1}$, in turn, is given by the moment equation

$$J_{\theta 1} = - e \int d^3 \underset{\sim}{p}\, v_\theta\, f_1 \tag{9}$$

where v_θ is the azimuthal electron velocity. To complete the analysis, the perturbed distribution function f_1 is given by the orbit integral

$$f_1 = e \int_{-\infty}^{t} dt' \left(\underset{\sim}{E}_1' + \frac{1}{c}\, \underset{\sim}{v}' \times \underset{\sim}{B}'\right) \cdot \frac{\partial f_o}{\partial \underset{\sim}{p}'} \quad , \tag{10}$$

where prime (') refers to the quantity along the equilibrium orbit $\underset{\sim}{x}'$ and $\underset{\sim}{p}'$ at time t'. First we note that, outside the beam (i.e. $\underset{\sim}{J}_1 = 0$), the solution to Eq. (8) is readily obtained. Namely

$$E_{\theta 1} = \begin{cases} C_1 J_1 (p_1 r) \ , & 0 \le r < R_- \\ C_2 J_1 (p_1 r) + C_3 N_1 (p_1 r), & R_+ < r \le R_w \\ C_4 J_1 (p_\varepsilon r) + C_5 N_1 (p_\varepsilon r) \ , & R_w \le r \le R_c \end{cases} \tag{11}$$

with the remaining components B_{z1} and B_{r1} given by Eq. (8). Here

$$\begin{aligned} c^2 p_1^2 &\equiv \omega^2 - c^2 k^2 \quad , \\ c^2 p_\varepsilon^2 &\equiv \omega^2 \varepsilon - c^2 k^2 \quad , \end{aligned} \tag{12}$$

and J_ℓ and N_ℓ refer to the first and the second kind of Bessel function of order ℓ. The contribution of the electron beam is represented by the integration of Eq. (8) over the beam region, viz.

$$B_{z1}(R_+) - B_{z1}(R_-) - \frac{i}{\omega c} p_1^2 \int_{R_-}^{R_+} E_{\theta 1}\, dr = -\frac{4\pi}{c} \int_{R_-}^{R_+} J_{\theta 1}\, dr \qquad (13)$$

Using the thin beam approximation [Eqs. (4)-(5)], we replace the left hand side of Eq. (13) by the jump condition on B_{z1} at R_o, but fully account for the orbit integral and the source equation [Eqs. (9)-(10)] in calculating the current contribution on the right hand side of Eq. (13). The appropriate boundary conditions uniquely determine the coefficients C's in Eq. (11), resulting in the desired dispersion relation. The necessary boundary conditons are: $E_{\theta 1}(R_c) = 0$ on the conducting wall, the continuity of $E_{\theta 1}(R_w)$ and $B_{z1}(R_w)$ on the inner radius of the dielectric material, and $E_{\theta 1}(R_-) \simeq E_{\theta 1}(R_+) \simeq E_{\theta 1}(R_o)$ and the jump condition on B_{z1} [Eq. (13)] at $R_o \simeq R_+ \simeq R_-$ via the thin beam assumption [Eq. (5)]. The orbit integral (10) and the subsequent calculations on the current contribution in Eq. (13) are tedious (we refer the detail to Ref. 10), and it is sufficient to say that the simple equilibrium fields [Eq. (3)] and the symmetry in θ and z greatly simplify the problem. We also add that in evaluating Eq. (10), use is made of the integral contour consisting of the real axis and the lower half circle in the complex p_z - plane.

It is noteworthy to compare this procedure of matching the boundary conditons with the waveguide approximation method used elsewhere.[11-13] It is assumed in the waveguide approximation that the field expression [Eq. (11)] is given by $J_1(\tilde{p}r)$ throughout the cross section where $c^2\tilde{p}^2 = \omega_G^2 - c^2k^2$. Here ω_G is the waveguide mode with absence of the electron beam. It is obvious that this approximation is valid only when the eigenfrequency ω is nearly equal to the free (without the beam) waveguide frequency ω_G. In view of the fact that the unstable mode is sup-

ported by the beam mode (see Sec. III), the validity of the waveguide approximation is guaranteed only for the beam-waveguide synchronous region. It cannot describe, as an extreme counter-example, the short wavelength mode (see Sec. III and VI) where the unstable mode is not the beam-waveguide interaction and indeed the field structure [Eq. (11)] is far different from $J_1(\tilde{p}\, r)$ (see Sec. III). Since, in our approach, the field profile is not apriori given but is determined as a result of the dispersion relation, it is applicable for arbitrary region including the short wavelength mode range.

We finally give the resulting dispersion relation for the azimuthally symmetric TE mode.

$$B = \frac{B_N}{B_D} = - \frac{\nu \beta_\perp^2}{2\hat{\gamma} R_o^2 \left[\omega - \omega_B + i\,|k| c\, \beta_z \hat{\gamma}\, \Delta / \gamma_z^3\right]^2} \quad . \tag{14}$$

Here the Doppler-shifted beam mode ω_B is defined by

$$\omega_B = k\, c\, \beta_z + \omega_c / \hat{\gamma} \quad , \tag{15}$$

and the wave admittance[8-10] is given by

$$\begin{aligned} B_N &= 2B_1 \\ B_D &= - \pi x_o^2 J_1(x_o) \left[J_1(x_o) B_2 - N_1(x_o) B_1\right] \quad , \\ B_1 &= J_1(y_c) A_{NJ}(y_w, x_w) - N_1(y_c) A_{JJ}(y_w, x_w) \quad , \\ B_2 &= J_1(y_c) A_{NN}(y_w, x_w) - N_1(y_c) A_{JN}(y_w, x_w), \end{aligned} \tag{16}$$

where

$$A_{PQ}(y_w, x_w) \equiv y_w P_o(y_w) Q_1(x_w) - x_w Q_o(x_w) P_1(y_w) \tag{17}$$

with P and Q standing for J or N.

Also,

$$\begin{Bmatrix} y_c^2 \\ y_w^2 \end{Bmatrix} = p_\varepsilon^2 \begin{Bmatrix} R_c^2 \\ R_w^2 \end{Bmatrix} \quad , \quad \begin{Bmatrix} x_w^2 \\ x_o^2 \end{Bmatrix} = p_1^2 \begin{Bmatrix} R_w^2 \\ R_o^2 \end{Bmatrix} \quad , \tag{18}$$

where p_1^2 and p_ε^2 are defined by Eq. (12), and $\gamma_z = (1-\beta_z^2)^{-\frac{1}{2}}$. It is understood that when $p^2 = -q^2$ is negative, the Bessel functions J and N become

$$
\begin{aligned}
J_o\,(pr) &= I_o\,(qr) \quad , \\
J_1\,(pr) &= i\,I_1\,(qr) \quad , \\
N_o\,(pr) &= -\frac{2}{\pi} K_o\,(qr) + i\,I_o\,(qr) \quad , \\
N_1\,(pr) &= -\,I_1\,(qr) + i\,\frac{2}{\pi} K_1\,(qr) \quad ,
\end{aligned}
\tag{19}
$$

where I_ℓ and K_ℓ refer to the first and the second kind of modified Bessel function. We mention here that the denominator of the wave admittance, B_D is directly proportional to the electric field at the beam location [i.e. $B_D \propto E_{3l}\,(R_o)$] whereas the numerator, B_N measures the degree of the synchronization between the waveguide frequency and the eigenfrequency. Especially we note that when $\nu=0$ (i.e., without the beam), $B_N = 0$ is the solution of Eq. (14), corresponding to the free waveguide dispersion equation. Moreover, when $R_c = R_w$ or $\varepsilon = 1$, the dispersion relation Eq. (14) is reduced to that for a simple waveguide gyrotron.[8]

In the next section we will analyze the dispersion relation Eq. (14) both analytically and numerically for a broad range of the system parameters in the entire spectrum of ω and k. Only unstable modes are investigated for the amplifier application.

III. CHARACTERISTICS OF UNSTABLE MODES

In this section we will derive an approximate dispersion relation for the unstable modes by making use of the tenuous beam assumption, identify three unstable modes, and examine the characteristics of each mode by analyzing this dispersion relation. Also discussed in this section is the general dependency of the growth rate on the axial momentum spread.

Making use of the fact that the applied frequency ω is nearly resonant with the beam mode ω_B (i.e., $|\omega - \omega_B| << \omega_c/\hat{\gamma}$) in order to be unstable, we can Taylor expand the wave admittance B by

$$B \simeq B(\omega_B) + B'(\omega_B)\,\chi \quad , \tag{20}$$

where B' stands for $(-1/c\beta_z)(\partial B/\partial k)$ at $k = (\omega - 1/\hat{\gamma})/c\beta_z$, and

$$\chi = \omega - kc\beta_z - \omega_c/\hat{\gamma} = \omega - \omega_B \tag{21}$$

refers to the eigenfrequency shift. Then the dispersion relation (14) becomes

$$[B'(\omega_B)\,\chi + B(\omega_B)]\,[\chi - i|k|c\beta_z\,\hat{\gamma}\Delta/\gamma_z^3]^2 = -\frac{\nu\beta_\perp^2}{2\hat{\gamma}R_o^2} \quad , \tag{22}$$

which is cubic in χ with the coefficients all known. Only the root with positive imaginary part (i.e., $\chi_i > 0$) corresponding to a growing mode, is selected.

Since the axial momentum spread (Δ) generally reduces the growth rate, we first investigate the stability properties for a cold ($\Delta=0$) beam case. From the property of a cubic equation, the necessary and the sufficient condition for the instability (i.e. $\chi_i > 0$) is given by

$$B(\omega_B) > -\frac{3}{2}\left[\frac{\nu\beta_\perp^2}{\hat{\gamma}R_o^2}\{B'(\omega_B)\}^2\right]^{1/3} \quad , \tag{23}$$

with the maximum growth rate found to be

$$\chi_i^{max} = \tfrac{1}{2}\left[\frac{\nu\beta_\perp^2}{2\hat{\gamma}R_o^2|B'(\omega_B)|}\right]^{1/3} \quad , \tag{24}$$

when

$$B(\omega_B) = 0 \quad . \tag{25}$$

It is interesting to examine the condition for the maximum growth rate [Eq. (25)] more carefully. From Eq. (14) we note that the optimum condition (25) can be achieved by following:

$$\text{(a) } B_N(\omega_B) = 0 \quad , \qquad \text{(b) } B_D(\omega_B) \to \infty \quad . \tag{26}$$

The case (a) corresponds to the synchronous interaction of the eigenmode with the free waveguide mode ($B_N = 0$ is the dispersion relation for the free waveguide mode), while the case (b) represents the perturbed electric field being highly localized at the beam location [i.e. $E_{\theta 1}(R_o) \sim \delta(r-R_o)$]. In the first case, the presence of the electron beam hardly perturbs the free waveguide fields so that the waveguide-beam mode coupling is most efficiently achieved. On the other hand, in the second case, the beam perturbs the waveguide so drastically that all the available charge bunching force is concentrated at the beam location. It is worthwhile to point out, as done in Sec. II, that the method of the wave impedance matching is valid even for the case (b), whereas the waveguide approximation is obviously inadequate to predict the case (b).

Analytical examinations of the dispersion relation (20) yield important results. By using small argument expansion when $p_1^2 \to 0$ [Eq. (12)], it can be shown that near the wavenumber k_c defined by

$$k_c = \frac{\omega_c}{\hat{\gamma} c(1-\beta_z)} \quad , \tag{27}$$

such that $\omega_B(k_c) = ck_c$, the mode is absolutely stable [$B(\omega_B) \propto 1/p_1^2 \to \infty$]. This is due to the fact that for $k = k_c$ (where the phase velocity $v_{ph} = \omega/k$ is equal to c), the electric field [Eq. (11)] at the beam location $E_{\theta 1}(R_o)$ is zero. In fact we can show that for $k = k_c$,

all the perturbed fields vanish. Since there is no electric field to derive the instability, the mode is stable. This fact remains true regardless of the other parameters. This stable mode at k_c provides a distinctive stability boundary between the fast ($v_{ph} > c$) and the slow ($v_{ph} < c$) wave modes. On the other hand, near the wavenumber $k = k_c^\varepsilon$ defined by

$$k_c^\varepsilon = \frac{\omega_c \varepsilon^{\frac{1}{2}}}{\hat{\gamma} c (1-\varepsilon^{\frac{1}{2}}\beta_z)} \quad , \tag{28}$$

characterized by $\omega_B(k_c^\varepsilon) = c\, k_c^\varepsilon/\varepsilon^{\frac{1}{2}}$, the wave admittance B (ω_B) is a positive value corresponding to a growing mode [Eq. (23)]. In this regard, there is no distinctive stability boundary when the mode phase velocity changes from $v_{ph} > c\varepsilon^{-\frac{1}{2}}$ to $v_{ph} < c\varepsilon^{-\frac{1}{2}}$.

In Fig. 2, a schematic growth rate (broken line) vs. k is plotted. Also shown in Fig. 2 are the real frequencies (solid lines) for the beam mode ω_B[Eq. (15)], the waveguide mode ω_G [the solution of $B_N = 0$, Eq. (14)], the free space mode ck, and the free dielectric mode $ck/\varepsilon^{\frac{1}{2}}$. The beam mode ω_B intersects with ck and $ck/\varepsilon^{\frac{1}{2}}$ at k_c [Eq. (27)] and k_c^ε [Eq. (28)], respectively. The growth rate curve shows that there are two distinctive regions; the fast wave ($\omega > ck$) and the slow wave ($\omega < ck$) separated by a stable band near $\omega = ck$ (i.e., near k_c) as expected. The growth rate for the slow wave reaches a maximum for $k < k_c^\varepsilon$ reduces somewhat and then increases (Fig. 2), thus exhibiting two maxima, one at $k < k_c^\varepsilon$ and the other as k approaches infinity. We identify these three unstable modes as the <u>long wavelength mode</u> (LWM) for $k < k_c$ (i.e. $v_{ph} > c$), the <u>intermediate wavelength mode</u> (IWM) for $k_c < k < k_c^\varepsilon$ (i.e. $c > v_{ph} > c\varepsilon^{-\frac{1}{2}}$) and the <u>short wavelength mode</u> (SWM) for $k > k_c^\varepsilon$ (i.e. $v_{ph} < c\varepsilon^{-\frac{1}{2}}$) according to their wavelength magnitudes.

It is found that while both the LWM and IWM unstable modes may disappear depending on the dielectric parameters (ε, R_w, R_c), the SWM is present

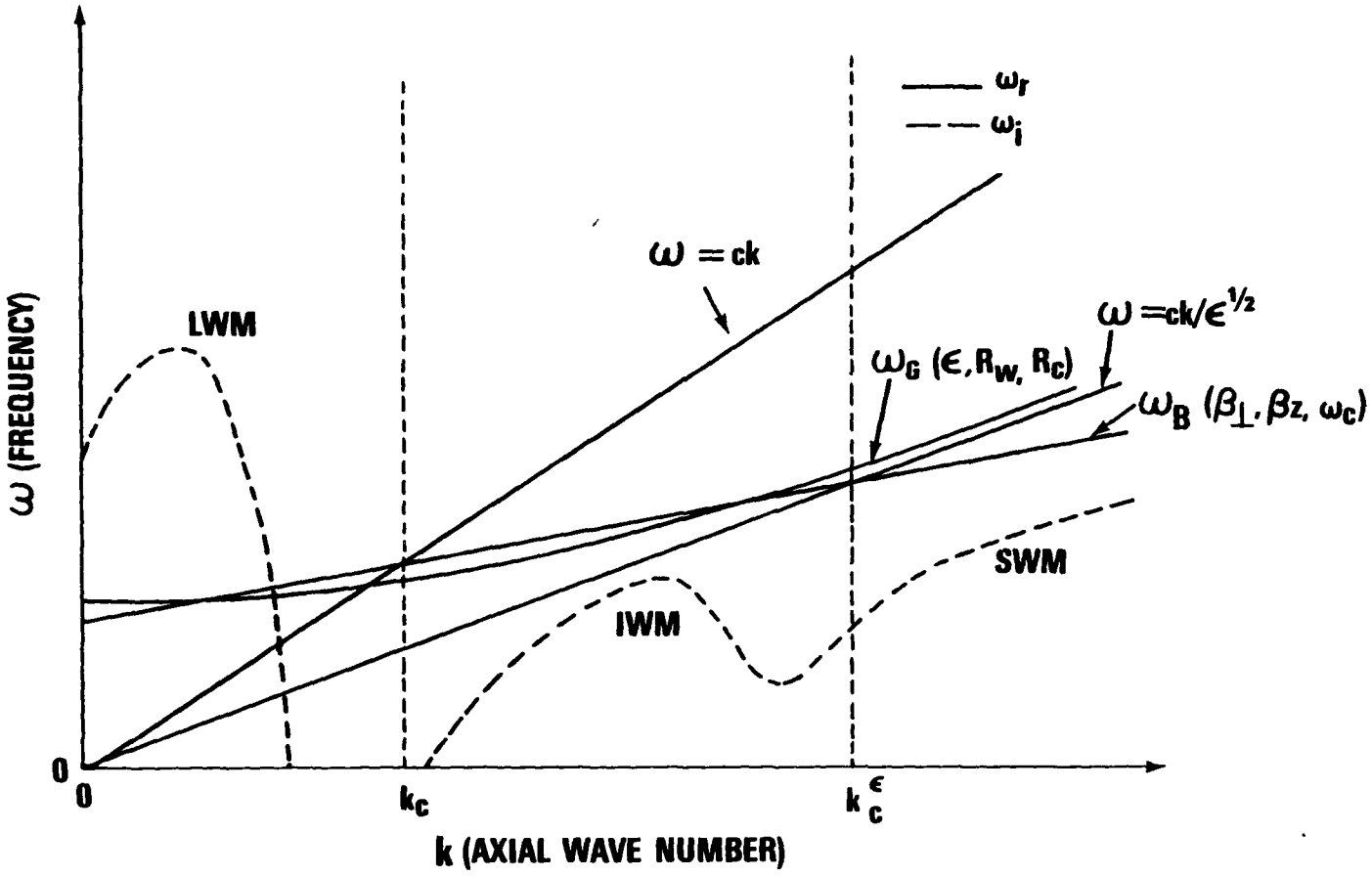

Fig. 2 — Schematic dispersion and gain curves vs. the axial wave number. The dispersion curves (solid) for the beam mode (ω_B), the dielectric waveguide mode (ω_G), and the two characteristic speeds (ck and $ck/\epsilon^{1/2}$) are shown. The gain curve (broken) shows three (LWM, IWM, and SWM) identified by the axial wave number. The distinguishing wave numbers k_c and k_c^ϵ are the intersecting points of $\omega = \omega_B$ with $\omega = ck$ and $\omega = ck/\epsilon^{1/2}$ respectively.

regardless of these parameters. Both the LWM and the IWM are originated from the unstable coupling of the beam mode ω_B with the waveguide mode ω_G. On the other hand, the instability of the SWM is driven by the highly localized electric field near the beam location. In fact the examination of the wave admittance shows that the appreciable gain for the LWM and the IWM occurs at $B_N \approx 0$ [Eq. (26-a)], whereas that for the SWM occurs at $B_D \to \infty$ [Eq. (26-b)]. From a simple waveguide (i.e., without the dielectric load, see Sec. VI), we find the SWM is not confined within $k > k_c^\varepsilon$, but it starts from near $k = k_c$. The presence of the dielectric load, when its parameters are properly adjusted, enhances the IWM unstable modes at $k \gtrsim k_c$ thereby overwhelming the small gain due to the SWM there. In this regard, the IWM unstable mode is coexisting with the SWM unstable mode. However, the growth rate due to the SWM at $k_c < k < k_c^\varepsilon$ is usually very small compared to that due to the IWM, and we can safely call this mode pure IWM.

Throughout the remainder of this paper, we assume the following beam parameters.

$$\beta_\perp = 0.40, \ \beta_z = 0.20, \ \nu = 0.002 \ , \tag{29}$$

corresponding to 60.3 KV of the anode voltage and 6.8 Amp. of the total axial current. For future reference, we also define

$$R_o^o = 2.017 \ c/\omega_c \ , \ R_c^o = 4.197 \ c/\omega_c \ . \tag{30}$$

It can be shown that R_o° and R_c° are the optimized beam center and the conducting wall locations when the dielectric is absent.[11,12] With the parameters in Eq. (29), it is found that the optimum ε values are ~ 5, ~ 15, and $= 1$ for the LWM, IWM, and SWM, respectively, and the maximum growth rates, normalized by its real frequency (χ_i/ω_r), are $\sim 1.8\%$, $\sim 0.8\%$, and $\sim 0.4\%$ for the LWM, IWM, and SWM, respectively.

So far we have discussed three unstable modes for the cold beam (Δ=0). The bandwidth, however, is primarily determined by the axial momentum spread. Before we discuss the spread effect for the individual modes (see next three sections), we will briefly mention the general dependency of the gain on the spread. From Eq. (22), the axial momentum spread that absolutely stabilizes the growth is given by[14]

$$\Delta_{max} \sim \chi_i|_{\Delta=0}/(|k|\ c\beta_z) \quad . \tag{31}$$

Evidently the degree of reduction in the gain due to the spread is the highest for the SWM, intermediate for the IWM, and the lowest for the LWM. With parameters in Eq. (29), Δ_{max} is >30%, ~10%, or ~2% for the LWM, IWM, or SWM, respectively.

In this section we found that there exist three unstable modes for the azimuthally symmetric, dielectric TE perturbations; the long wavelength mode, the intermediate wavelength mode and the short wavelength mode characterized by their wavelength magnitudes. Also we found the different instability mechanisms for these modes. In the next three sections we will scan the whole parameter space (ε, R_w, R_c, R_o) to obtain the optimum conditions for the wide bandwidth and examine the dependency of the gain on the axial momentum spread for these three unstable modes.

In order to avoid confusion, we list frequently quoted names for the three unstable modes. Both the SWM and the dielectric loaded LWM have not been previously examined. The simple waveguide (ε=1) LWM is often called as the "Gyro-TWA" and as the "fast wave." The IWM is frequently called as the "slow wave," which is confusing in view of the presence of the SWM. The IWM is also called as the "Weibel mode." The SWM is, without any valid analysis, often called as the "Weibel mode" and as the "whistler mode." These are tabulated in Table I.

Table I — Other terminologies for three modes

LWM	IWM	SWM
o Fast Wave	o Slow Wave	o Whistler Mode
o Gyro-TWA	o Weibel Mode	o Weibel Mode

IV. LONG WAVELENGTH MODE (LWM)

The long wavelength mode (LWM) is a fast wave interaction between the dielectric waveguide and the beam modes, and is separated from the intermediate wavelength mode (IWM) by a stable region near k_c (see Fig. 2). Unlike the IWM, always mixed with the short wavelength mode (SWM), the LWM unstable mode has its stability boundary. In Fig. 3 the stability boundaries for the LWM in the R_w-R_c parameter space are presented for several values of the dielectric constant ε. Both the conducting wall radius R_c and the dielectric inner radius R_w are normalized to R_c° [Eq. (30)], which is the optimum conducting wall radius without the dielectric load. The LWM mode is stable above the boundary and may be unstable below it. The curves are obtained for the beam parameters in Eq. (29), assuming zero axial momentum spread (Δ=0). Evidently, the thickness of the dielectric material, represented by the vertical distance from the $R_w = R_c$ line to the boundary curve, decreases as ε increases in order to be unstable. Moreover, we also note from Fig. 3 that the thick dielectric loading requires reduction in the conducting wall size. Stability properties are more sensitive to a small dielectric constant.

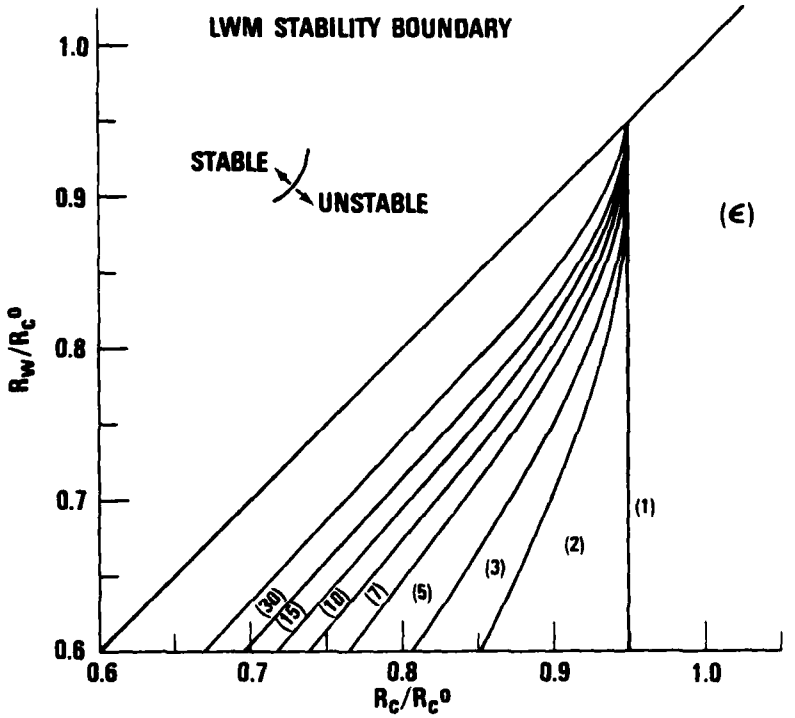

Fig. 3 — Stability boundary of the long wavelength mode in the R_w-R_c space. Both the inner wall radius (R_w) and the conducting wall radius (R_c) are normalized by R_c° in Eq. (30). For given dielectric material (ϵ), the LWM is unstable below the stability boundary.

In Fig. 4, the maximum gain contours for the LWM are presented in the R_w-R_c space for various values of ϵ. Comparing Fig. 4 with Fig. 3, it is found that the maximum gain occurs at a deep inside the stability boundary as R_c increases and ϵ decreases. Shown in Fig. 5 are the maximum growth rates vs. R_c along its maximum gain contour given in Fig. 4. The possible maximum gain is a decreasing function of both ϵ and R_c, reaching saturation at higher ϵ and lower R_c. It is also noted from Figs. 3-5 that both the instability boundary and the maximum gain curves are insensitive to the dielectric thickness (R_c-R_w) for $\epsilon \gtrsim 10$ (also see the discussion in Sec. V).

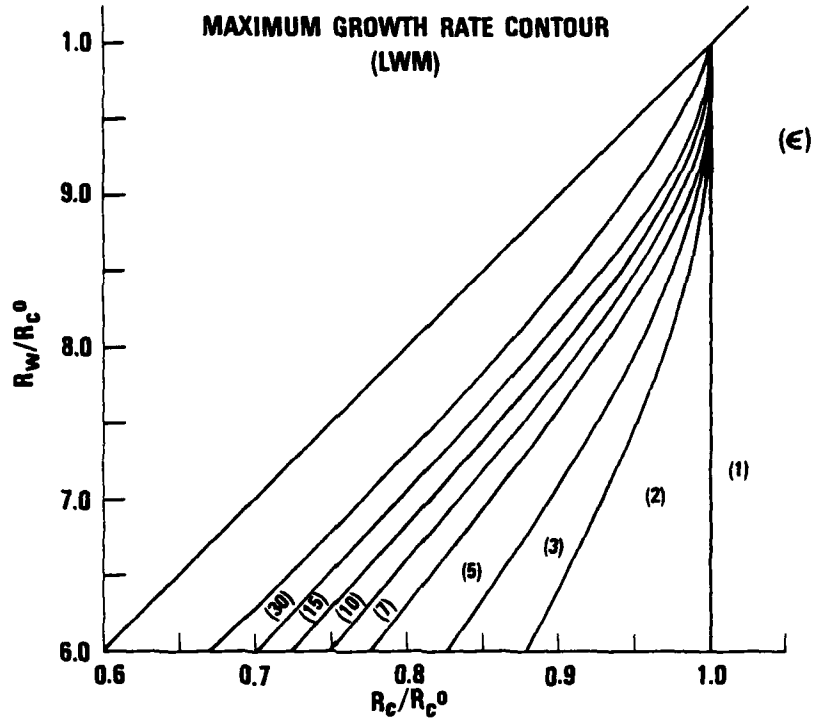

Fig. 4 — Maximum linear gain contour for the long wavelength mode in the R_w-R_c parameter space.

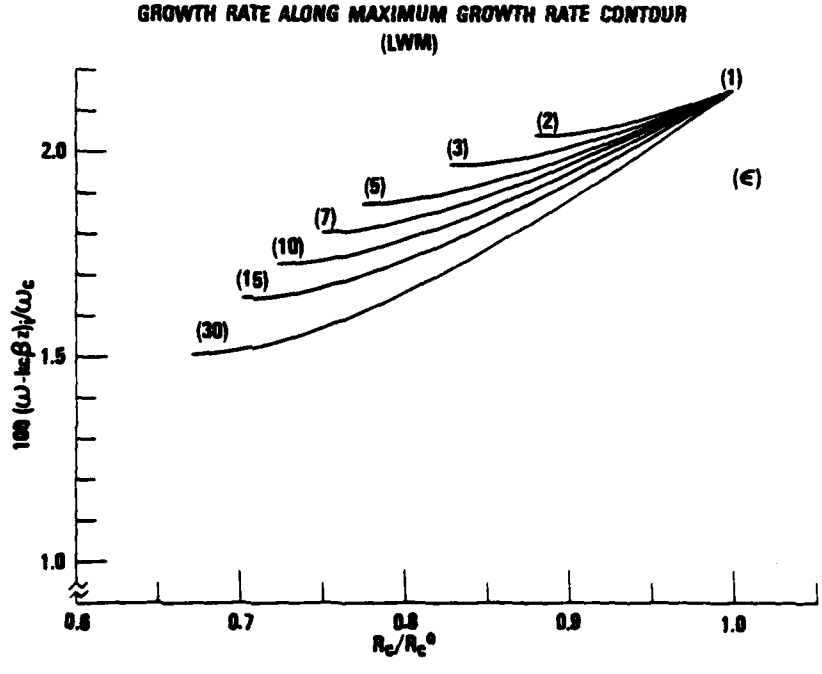

Fig. 5 — Growth rate along the maximum gain contour given in Fig. 4.

The bandwidth of the LWM for a cold beam ($\Delta=0$) is limited from the facts that for $k = k_c$, the transverse fields for $0 \leq r \leq R_o$ vanish (see Sec. III), and that for some system parameters, the beam mode never synchronizes the waveguide mode. From the numerical calculation, it is found that the optimum bandwidth contours in the R_w-R_c space are almost identical to those of the maximum growth rate in Fig. 4. However, the bandwidth increases as R_c increases, which is contrast with the R_c-dependence of the growth rate (see Fig. 5). We also note that the bandwidth is an increasing function of ε up to $\varepsilon=5$, beyond which it is actually decreasing as ε further increases. This is due to the difficulty in achieving the beam-waveguide synchronization within the LWM range at higher ε (see Sec. V). It appears that the optimum dielectric constant ε for the LWM is given by $\sim 1/\beta_z$. Since the electric field tends to concentrate within the dielectric material, the growth rate and the bandwidth increases as the beam center R_o approaches its physical limit of R_w-r_L. This R_o optimization condition restricts the bandwidth broadening effect of the smaller conducting wall radius. Therefore, we conclude that the optimum parameters for the wide band operation of the LWM with a cold beam are given by $\varepsilon=5$, $R_c = 0.80\ R_c^\circ$, $R_w = 0.62\ R_c^\circ$ and $R_o = R_w - r_L$.

The most important parameter to determine the bandwidth is the axial momentum spread. Although the LWM suffers least from the spread among the three unstable modes, the stability dependency on the spread changes the picture of the optimum conditions for the wide band operation. The optimum wall radius R_c increases from R_o° [Eq. (30)] to R_c° [Eq. (30)] as the axial momentum spread increases. Shown in Fig. 6 are plots of the growth rates vs. k for $\varepsilon = 1$, $R_c = 1.008R_c^\circ$, $R_o = 0.481\ R_c^\circ$ (broken lines), and $\varepsilon = 5$, $R_c = 0.800R_c^\circ$, $R_w = 0.624R_c^\circ$, $R_o = 0.524R_c^\circ$ (solid lines) at

several different values of the momentum spread Δ. Obviously from Fig. 6, for a small spread ($\Delta \lesssim 3\%$), the bandwidth for $\varepsilon = 5$ is broader than that for $\varepsilon = 1$. However, in contrast to the broken lines in Fig. 6, the bandwidth for $\varepsilon = 5$ reduces rapidly as the spread increases (also see the discussions in Sec. VII).

In this section we have performed parametric investigations on the LWM unstable modes. It is found that for a small spread the dielectric LWM with $\varepsilon = 5$ is suitable for the wide band operation. On the other hand, for a large spread the simple waveguide (with $\varepsilon = 1$) is preferable. Moreover, the beam center location is preferable at near the inner wall of the dielectric for a small spread, whereas its optimum position is R_o° [Eq. (30)] for a large spread. We also found that the gain for the LWM with the dielectric loading is approximately the same as that for the simple waveguide LWM.

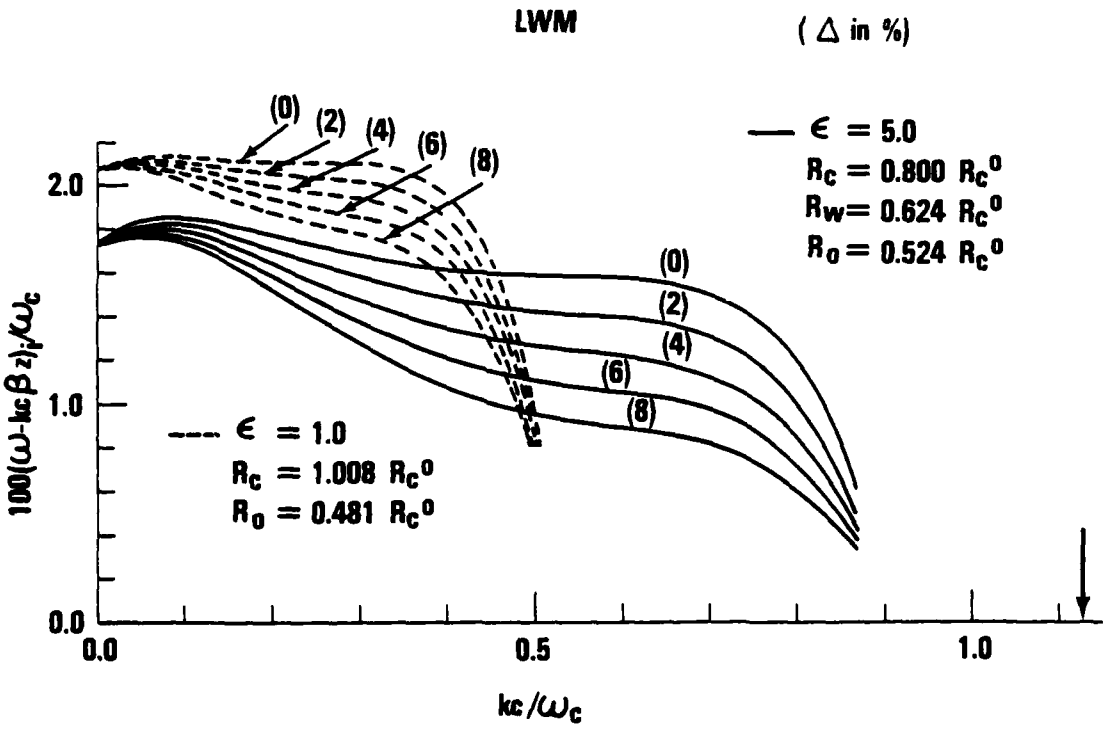

Fig. 6 — Gain curves of the long wavelength mode for several values of the axial momentum spread. The solid curves are for the optimized dielectric gyrotron, and the broken for the optimized gyrotron without the dielectric load. The arrow refers to k_c [Eq. (27)], the limit of the LWM.

V. INTERMEDIATE WAVELENGTH MODE (IWM)

The intermediate wavelength mode is characterized by the phase velocity v_{ph} in the range $c > v_{ph} > c\varepsilon^{-1/2}$ [or $k_c < k < k_c^{\varepsilon}$, Eqs. (27)-(28)]. In this region we note $p_1^2 < 0$ and $p_\varepsilon^2 > 0$ [Eq. (12)], so that the Bessel functions with argument x's become the modified Bessel functions according to Eq. (19). As discussed before, the IWM always exists together with the short wavelength mode. When the beam mode is considerably out of synchronization with the waveguide mode, the IWM disappears completely, leaving the SWM only. In this regard, there is no means to define the stability boundary for the IWM. It is, however, safe to say that the growth rate contributed by the SWM in the range $k_c < k < k_c^{\varepsilon}$ is usually negligible in comparison with that by the IWM.

Like the long wavelength mode, the unstable IWM is driven by the coupling between the beam and the waveguide modes. The growth rate and the bandwidth of the IWM are, therefore, optimized when the dispersion curve of the beam mode $\omega = \omega_B$ is tangential to that of the dielectric waveguide mode $\omega = \omega_G$ (see Fig. 2). The parametric conditions to make the beam mode graze the dielectric waveguide mode are shown in Fig. 7. The dielectric constant ε [Fig. 7(a)] and the corresponding conductor radius R_c [Fig. 7(b)] versus the wave number k_g where the grazing takes place are given for several values of the thickness parameters R_w/R_c. When the relative thickness of the dielectric material is small (i.e., $R_w/R_c \to 1$), the beam mode grazes the waveguide mode at two different wave numbers (k_g) at high ε. However, for a thicker dielectric material (i.e., $R_w/R_c \to 0$), the modes graze each other at only one wave number k_g for all ε. We also note that at $\varepsilon \simeq 15 \sim 16$ for $\beta_z = 0.2$, the ε- curve and the corresponding R_c-curve are almost flat in the k_g space. That is, at this particular ε, the beam mode grazes or nearly grazes the waveguide mode for a broad range of the axial wave number

in the IWM region. Thus we find that for our beam parameters [Eq. (29)], the beam-waveguide synchronous region is significantly stretched when $\varepsilon = 15 \sim 16$, $R_w/R_c = 0.90 \sim 0.80$, and $R_c/R_c^\circ = 0.70 \sim 0.50$. It is also obvious from Fig. 7(a) that for a thick ($R_w/R_c \lesssim 0.75$) dielectric material with high dielectric constant ($\varepsilon \gtrsim 10$), the axial grazing wave number k_g is greater than k_c, thereby indicating that in these system parameters, the optimum gain and the bandwidth for the LWM are unattainable. This explains the insensitivity of the gain and the bandwidth of the LWM for high ε (see Sec. IV).

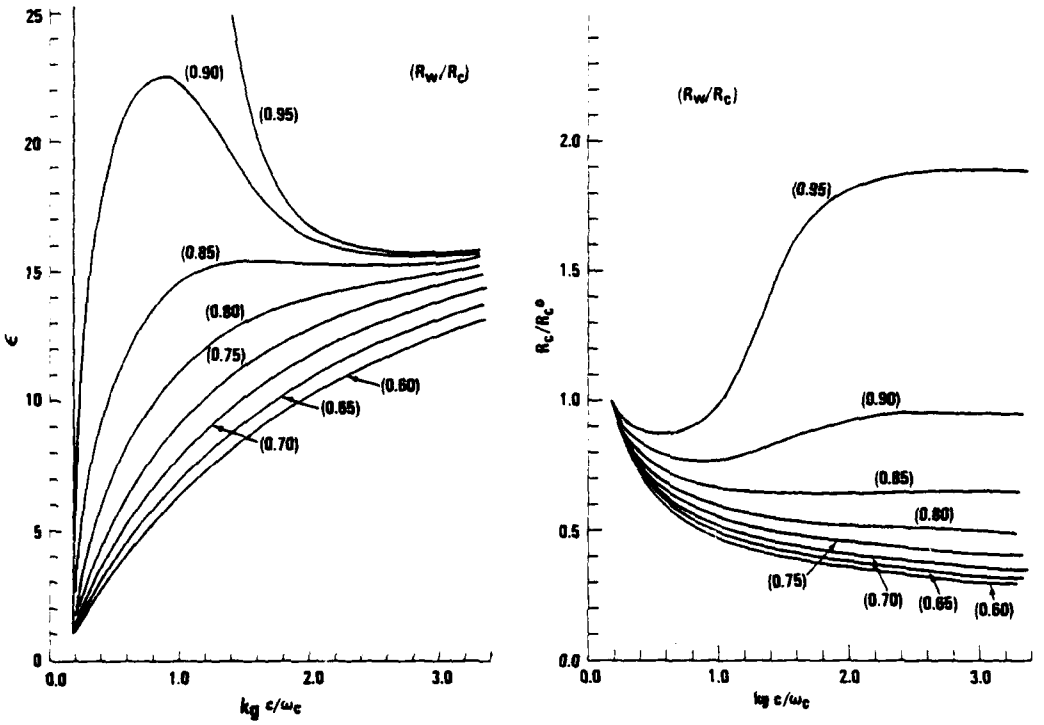

Fig. 7 — Conditions for the beam-waveguide mode grazing. (a) The dielectric constants at which the beam mode grazes the waveguide mode at k_g are shown for several values of R_w-R_c. (b) Corresponding conductor radii vs. k_g.

In order to illustrate the effect of the axial momentum spread on the stability behavior of the IWM, we present the plot of the growth rates vs. the wave number in Fig. 8. The parameters (ϵ = 15.2, R_c = 0.630 R_c°, R_w = 0.532 R_c°, R_o = 0.427 R_c°) are obtained from the optimization process with aid of Fig. 7. Since the electric fields tend to concentrate on the high ϵ dielectric layer, it is obvious that the growth rate increases as the beam location R_o approaches to R_w. In Fig. 8, the growth rate for the cold beam ($\Delta \approx 0$) increases monotonically increases as k increases from k = 3.5 ω_c/c (after the IWM maximum) to infinity, obviously indicating the SWM contribution. However, this SWM influence quickly disappears by introducing even a very small amount of the axial momentum spread ($\Delta \geq 2\%$).

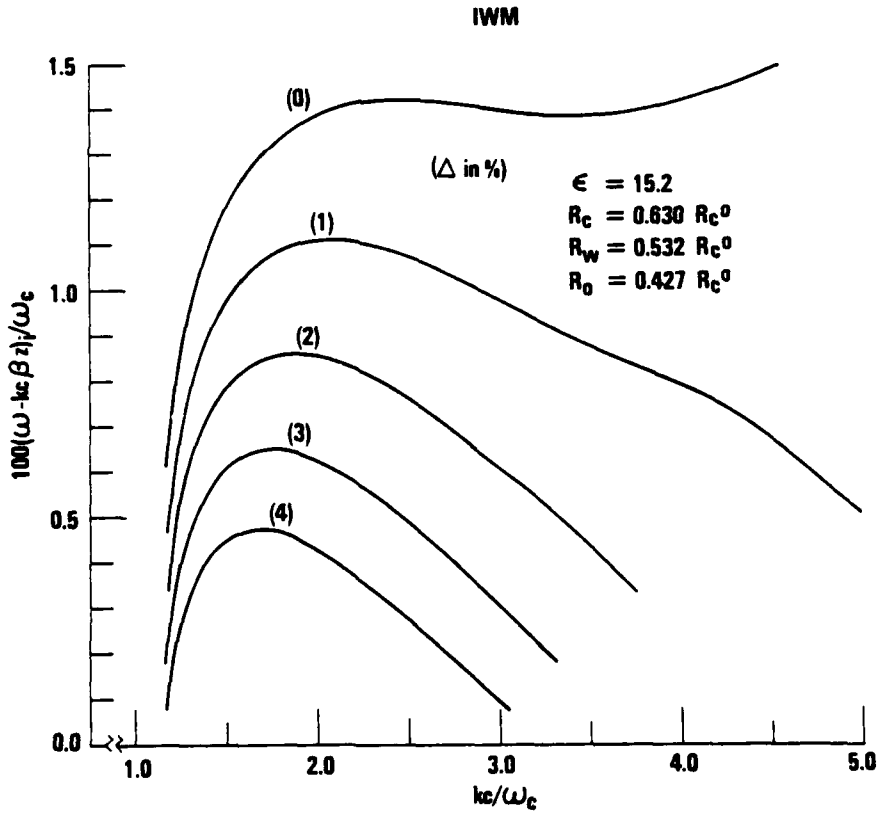

Fig. 8 — Plots of the growth rates for the optimized intermediate wavelength mode for several values of the axial momentum.

As the spread increases, the IWM gain decreases very rapidly and so does the bandwidth. (Numerical presentations are given in Sec. VII.) As discussed in Sec. III, the gain is more sensitive to the spread than that for the LWM. Unlike for the LWM, however, the optimization condition for the IWM does not change as the spread increases. It is also found that when the spread is greater than 10%, the gain for the IWM is completely wiped out, which is contrast comparing with >30% for the LWM.

VI. SHORT WAVELENGTH MODE (SWM)

The short wavelength mode appears when the phase velocity v_{ph} is less than c. However, due to the presence of the more dominant intermediate wavelength mode (see Sec. V), it is, for convenience, defined as the unstable modes with $v_{ph} < c\varepsilon^{-\frac{1}{2}}$ (or $k > k_c^{\varepsilon}$) when the dielectric is present. Unlike both the long and the intermediate wavelength modes, the SWM is originated from the acute localization of the electromagnetic fields at the beam location. In the SWM region the electron beam itself behaves like a high ε dielectric material and absorbs almost all of the fields inside. As discussed in Secs. III and V, the IWM is more prominent when the dielectric loading is present. Therefore, we will examine the SWM without the dielectric clad in this section.

It can be shown that for the cold beam ($\Delta = 0$) in a simple waveguide without a dielectric, the wave admittance $B(\omega_B)$ in Eq. (14) is always positive, and decreases to zero as k increases to infinity. According to the stability condition Eq. (23), the SWM is, therefore, always present unlike the LWM and the IWM. The gain χ_i is a monotonically increasing function of k with its asymptotic behavior given by $\chi_i \propto k^{\frac{1}{2}}$ Furthermore, the gain is found to be a monotonically decreasing function of the beam

center R_o and a monotonically increasing function of the conductor radius R_c. The present theory, however, breaks down as R_o approaches zero due to the assumption Eq. (4).

Figure 9 illustrates the SWM gain versus the axial wave number for various values of the axial momentum spread. As pointed out in Sec. III, the SWM is the most sensitive to the spread, completely disappearing when the spread is greater than 2%. Similarly the bandwidth is rapidly decreasing as the spread increases.

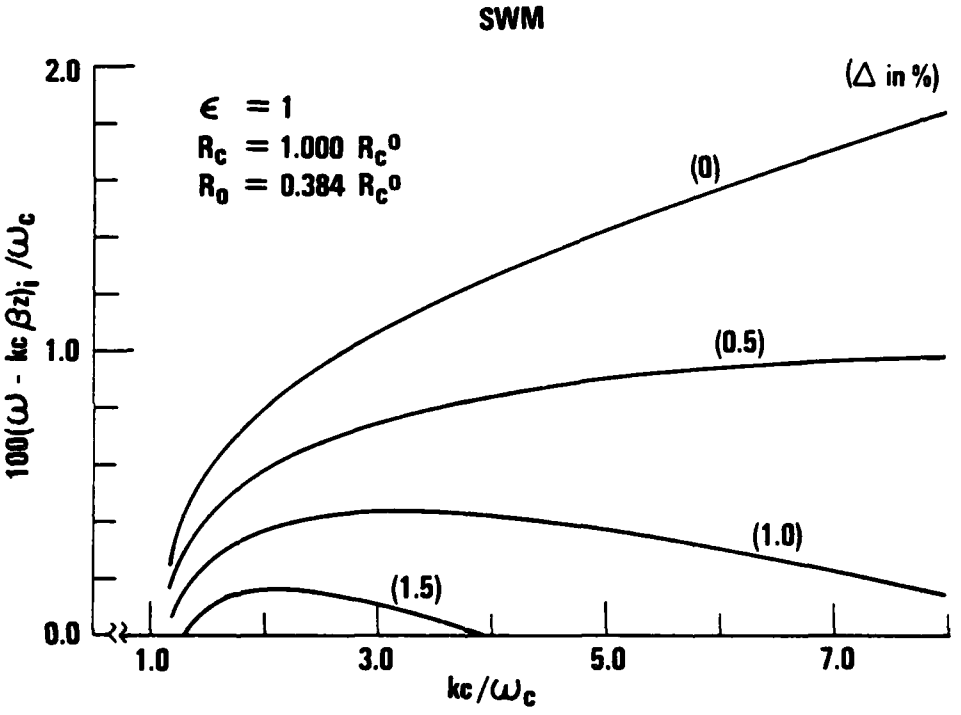

Fig. 9 — Plots of the growth rates for the optimized short wavelength mode for several values of the axial spread.

VII. COMPARISON OF THREE MODES

In the previous sections we have examined the three unstable modes existing in a dielectric loaded gyrotron. In this section we will compare these modes in terms of the bandwidth and the linear gain as the axial momentum spread of the beam is varied.

In Fig. 10, the bandwidth and the linear gain for the various modes, individually optimized are shown as a function of the axial velocity spread Δ. Here LWM^1 refer to the LWM without the dielectric shown by the broken line in Fig. 6; LWM^ε to the LWM with $\varepsilon = 5$ dielectric loading shown by the solid line in Fig. 6; IWM to the IWM with $\varepsilon = 15.2$ in Fig. 8; and SWM to the SWM with $\varepsilon = 1$ in Fig. 9. The bandwidth in Fig. 10 is defined by the full-width of the real frequency, at which the linear gain drops to exp $(-\frac{1}{2})$ of its maximum value, normalized by the mean frequency $\bar{\omega}$. The linear gain is also normalized by the mean frequency $\bar{\omega}$. It is apparent from Fig. 10 that for a small spread (Δ=1%), the bandwidth for the SWM (> 60%) is broadest, followed by the IWM ($\sim$ 45%), the dielectric LWM^ε ($\sim$ 16), and the simple LWM^1 ($\sim$ 12%). As the spread increases, the rate of the bandwidth reduction is the highest for the SWM, followed by the IWM, the dielectric LWM^ε and the simple LWM^1, which stays almost unchanged. For a large spread (Δ = 8%), the simple waveguide LWM^1 is wider in its bandwidth ($\sim$ 11% [illegible] on the dielectric LWM^ε ($\sim$8%), even wider than the IWM ($\sim$ 9%). We note [illegible] the plot of the normalized maximum growth rate versus Δ that the ratios of the linear gain to that of the LWM^1 is given by 0.85, 0.35, and 0.19 for the LWM^ε, IWM, and SWM, respectively, even for a very small momentum spread (Δ = 1%). Moreover, the linear gains for the IWM and SWM reduce very rapidly as the spread increases. On the other hand the LWM^1 and LWM^ε show insensitivity to the spread.

From Fig. 10, we conclude that, for a broad bandwidth operation, the SWM is desirable when the spread is less than 1% (with 60% bandwidth), the IWM for 1% <Δ< 7% (with 40 ∿ 25% bandwidth), and the LWM^1 for a Δ > 7% (with 10% bandwidth). If, however, the bandwidth is to be compromised with the linear gain, at small spread (Δ < 5%) the IWM is the one to choose, at moderate spread (5% <Δ<7%) the dielectric LWM^ϵ is better, and at large spread (Δ > 7%) the simple LWM^1 is desirable.

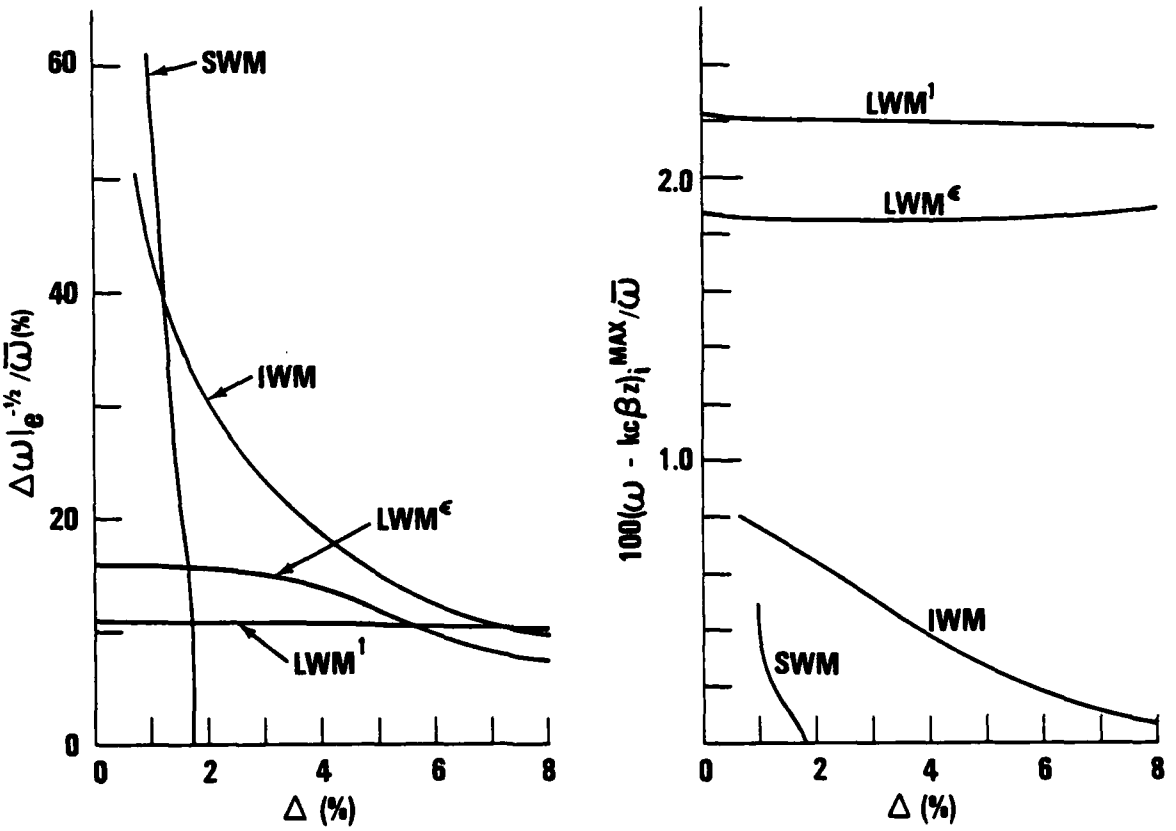

Fig. 10 — Plots of the bandwidth and the maximum growth rate vs. the axial momentum spread for the various modes. The LWM^1 and LWM^ϵ refer to the long wavelength modes in the waveguide without the dielectric (broken lines in Fig. 6) and with the dielectric (solid lines in Fig. 6), respectively. The IWM and SWM represent the intermediate (Fig. 8) and the short (Fig. 9) wavelength modes, respectively. For the definition of the bandwidth, see the text.

VIII. CONCLUSIONS

We have obtained and examined a linear dispersion relation for the azimuthally symmetric TE perturbation in a dielectric (ε) loaded gyrotron. It is found that there exist three unstable modes characterized by their phase velocities v_{ph}; the long wavelength mode (LWM, $v_{ph} > c$), the intermediate wavelength mode (IWM, $c > v_{ph} > c\varepsilon^{-1/2}$), and the short wavelength mode (SWM, $v_{ph} < c\varepsilon^{-1/2}$). Both the long and intermediate wavelength modes arise from the beam-waveguide mode coupling, whereas the short wavelength mode is driven by the highly localized fields at the beam location. The LWM is separated from the other modes by a stable region near $\omega = ck$, and the IWM appears always together with the SWM.

The optimum conditions on the physical parameters for a wide band operation are summarized in Table II for each mode. Here R_c° and R_o° are defined by Eq. (30) and refer to the optimum wall radius and beam center location, respectively, when the dielectric is absent.

Table II — Optimum parameters for three modes

	SPREAD	ε	R_c/R_c°	R_w/R_c	R_o
LWM	<5%	$\sim$5	$\sim$0.8	0.7$\sim$0.8	$\sim R_w$
	5 $\sim$30%	= 1	$\sim$1.0	—	R_o°
IWM	<10%	$\sim$15	$\sim$0.6	0.7$\sim$0.8	$\sim R_w$
SWM	<2%	= 1	>>1	—	$\to 0$

Preferable modes for a wide band operation in terms of the axial momentum spread are summarized in Table III. The modes with asterisk (*) are desired when the high gain is also needed.

Table III — Preferable mode for wide band operation

SPREAD	USE	ε	BANDWIDTH
<1%	SWM	≈1	>60%
	IWM*	∿15	>40%
1∿7%	IWM	∿15	40-25%
	LWM*	∿5	16-10%
>7%	LWM	=1	∿10%

*When high gain is also desired.

The presence of the short wavelength mode and the promising wide band capability of both the intermediate and short wavelength modes necessitate more rigorous understanding of the electron gun profile. Also needed are studies on how to excite these modes without significant energy loss (e.g., coupler, collector).

ACKNOWLEDGMENT

This research was supported in part by an Independent Research Fund at the Naval Surface Weapons Center, and in part by the Office of Naval Research and the Naval Electronic Systems Command.

REFERENCES

1. V.A. Flyagin, A.V. Gaponov, M.I. Petelin, and V.K. Yulpatov, IEEE Trans. Microwave Theory Tech. MTT-25, 514 (1977).
2. J.L. Hirschfield and V.L. Granatstein, IEEE Trans. Microwave Theory Tech. MTT-25, 528 (1977).
3. Also see the papers referred in Refs. 1 and 2.
4. J.R. Pierce, Traveling-Wave Tubes, (D. Van Nostrand Co., Inc., New York, 1950) Chap. 2.
5. A.K. Ganguly and K.R. Chu, NRL Memo. Rep. 4215 (1980).

6. J.M. Baird, S.Y. Park, K.R. Chu, H. Keren, and J.L. Hirshfield, Bull. Am. Phys. Soc. 25, 911 (1980).

7. J.Y. Choe, H.S. Uhm, and S. Ahn, Bull. Am. Phys. Soc. 25, 887 (1980).

8. H.S. Uhm, R.C. Davidson, and K.R. Chu, Phys. Fluids 21, 1866 (1978).

9. H.S. Uhm, R.C. Davidson, and K.R. Chu, Phys. Fluids 21, 1877 (1978).

10. H.S. Uhm and R.C. Davidson, Phys. Fluids 23, 2538 (1980).

11. K.R. Chu, Phys. Fluids 21, 2354 (1978).

12. J.Y. Choe and S. Ahn, NRL Memo. Rep. 4041 (1979); S. Ahn and J. Choe, IEEE Electron Device Lett. EDL-1, 8 (1980).

13. J.Y. Choe and S. Ahn, NRL Memo. Rep. 4035 (1979); J.Y. Choe and S. Ahn, IEEE Trans. Electron Devices ED-28, 166 (1981).

14. J.Y. Choe and S. Ahn, IEEE Trans. Electron Devices ED-27, 962 (1980).


DAT
ILM